PCCP

Accepted Manuscript

ROYAL SOCIETY OF CHEMISTRY

www.rsc.org/pccp

Cite this: DOI: 10.1039/c0xx00000x

www.rsc.org/xxxxxx

ARTICLE TYPE

Nonlinear absorption, nonlinear scattering, and optical limiting properties of MoS_2/ZnO composite-based organic glasses†

Bin Qu,[a,b] Qiuyun Ouyang,*[a] Xianbo Yu,[a] Wenhe Luo,[a] Lihong Qi,[a] and Yujin Chen*[a]

Received (in XXX, XXX) Xth XXXXXXXXX 20XX, Accepted Xth XXXXXXXXX 20XX

DOI: 10.1039/b000000x

MoS_2/ZnO composites were synthesized by a solution-based method. The scanning electron microscopy and transmission electron microscopy analysis demonstrated that ZnO nanoparticles with a size of about 4.5 nm were coated on the basal surface of MoS_2 nanosheets with expanded spacing of (002) plane. The MoS_2/ZnO composite-based poly(methyl methacrylate) (PMMA) organic glasses (MoS_2/ZnO/PMMA organic glasses) were prepared through a polymerization process. The nonlinear absorption (NLA), nonlinear scattering (NLS), and optical limiting (OL) properties of the MoS_2/ZnO/PMMA organic glasses with different amounts of MoS_2/ZnO were investigated by a modified Z-scan technique. Compared to MoS_2/PMMA and ZnO/PMMA organic glasses, the MoS_2/ZnO/PMMA organic glasses exhibited enhanced NLA, NLS, and OL properties, which were attributed to the interfacial charge transfer between MoS_2 nanosheets and ZnO nanoparticles, the layered structure of MoS_2 nanosheets, the small size effect of ZnO nanoparticles, and the local field effect. In addition, a changeover from saturable absorption (SA) to reverse saturable absorption (RSA) could be realized in the MoS_2/ZnO/PMMA organic glasses by adjusting the input energy. The total nonlinear extinction coefficient and response time of the MoS_2/ZnO/PMMA organic glasses could be up to 2380 cm GW^{-1} and several hundred picoseconds, respectively. Compared to the MoS_2 films, the MoS_2/ZnO/PMMA organic glasses have higher optical damage threshold, better mechanical strength and flexibility. Thus The MoS_2/ZnO/PMMA organic glasses are very promising for optical devices such as optical limiters, optical shutters, ultrafast lasers, and ultrafast optical switches.

1 Introduction

Molybdenum disulfide (MoS_2) is a typical two-dimensional (2D) layered material, in which hexagonal layers of Mo atoms are sandwiched between two layers of sulfur atoms (S).[1, 2] Due to its unique layered structure and relatively narrow band gap (1.2–1.9 eV),[3, 4] MoS_2 has been potential applications in optoelectronic fields such as photocatalysis,[5–9] photoluminescence,[10, 11] light-emitting diodes,[12] phototransistors,[13–15] optical limiters,[16, 17] ultra fast photonic devices,[18, 19] and solar cells.[20] However, for the single MoS_2 material, the intrinsic defects such as dislocations, stacking fault, the high recombination rate of the photo-generated electron-hole pairs, and the lack of effective emission sites,[6, 21] limit its practical applications in some fields. Recently, it has been reported that by combining MoS_2 with other materials, these drawbacks can be overcome to some degree.[22–26] For example, Combining MoS_2 with graphene, ZnO, TiO_2, and CdS can enhance photocatalytic activities,[6–9] nonlinear optical (NLO) properties,[17] and electrochemical performances, respectively.[22] MoS_2/carbon hybrid possesses high efficient platinum-free counter electrode for dye-sensitized solar cells.[23] MoS_2 blended with single-walled carbon nanotubes (SWNTs) to form novel composite thin films, which show strong electrochemical performance for lithium ion batteries.[24] Recently, MoS_2@ZnO nanoheterjunctions were fabricated and exhibited enhanced field emission properties.[6] However, up to now the NLO properties of the MoS_2/ZnO composite-based organic glasses has not been reported.

ZnO, as a wide semiconductor with a band gap of 3.37 eV and a high exciton binding energy of 60 meV, has been widely used in photocatalysis,[6] optical shutters,[27, 28] optical limiters,[29] heterojunction laser diodes, and UV lasers.[30] Due to its wide band gap structure, ZnO has been combined with graphene[28] or other semiconductors with narrower band gaps, including Cu_2S,[31] Cu_2O,[32] CdS,[33] CdSe,[34] etc., to enhance optoelectronic performances. In addition, it has been proved experimentally that both MoS_2 and ZnO have excellent NLO properties,[16–19, 27–30] Therefore, the MoS_2/ZnO composites may have enhanced NLO properties.

Herein, we synthesized MoS_2/ZnO composites by using a solution-based method. Then, the MoS_2/ZnO composites were dispersed in methyl methacrylate (MMA) to prepare an organic glass by a casting method, and the MMA was polymerized to poly(methyl methacrylate) (PMMA).[17, 28, 35] The nonlinear absorption (NLA), nonlinear scattering (NLS), and optical limiting (OL) properties of the MoS_2/ZnO/PMMA organic glasses were investigated by a modified Z-scan technique.[35] The MoS_2/ZnO/PMMA organic glasses exhibited enhanced NLA, NLS, and OL properties. In addition, a changeover from saturable absorption (SA) to reverse saturable absorption (RSA) could be realized in the MoS_2/ZnO/PMMA organic glasses by adjusting the input energy. The related mechanism was discussed.

2 Experimental section

2.1 Synthesis of MoS_2/ZnO composites

MoS_2 nanosheets were synthesized by a solution-based method.[36]

Simply, $(NH_4)_6Mo_7O_{24}\cdot 4H_2O$ (1 mmol) and thiourea (30 mmol) were dissolved in distilled water (35 mL) under vigorous stirring to form a homogeneous solution. After being stirred for 30 min, the solution was transferred into a 50 mL Teflon-lined stainless steel autoclave and maintained at 180°C for 24 h. The obtained products were collected by centrifugation, washed with distilled water and ethanol, and dried at 60°C under vacuum.

The MoS_2/ZnO composites were synthesized as the following. $Zn(CH_3COOH)_3\cdot H_2O$ (1.4 g) was dispersed in ethanol (250 mL). The mixture was heated at 80°C for 10 min in a water bath. Then $LiOH\cdot H_2O$ (0.4 g) was added the above the mixture. After sonication for 15 min at room temperature, MoS_2 nanosheets (30 mg) were added and sonication another 20 min. After stirring for 2.5 h at room temperature, the precipitates were separated by centrifugation, washed with absolute ethanol, and dried in a vacuum oven at 40°C for 24 h.

2.2 Fabrication of MoS_2/ZnO/PMMA organic glasses

The MoS_2/ZnO/PMMA organic glasses were prepared via the following steps. (1) 2,2′-Azobis(isobutyronitrile) (0.03 g) was dispersed in MMA (10.35 g), and then an appropriate amount of MoS_2/ZnO composite was added. After sonication for 10 min and stirring for another 40 min at room temperature, the mixture was heated at 75°C for 30–35 min in a water bath, until the formation of a jelly-like material was observed. (2) The jelly-like material was then cast into a clean glass mould. The mould was sealed well and dried at 45°C for 10 h; then, it was cooled gradually to room temperature to obtain the MoS_2/ZnO/PMMA organic glass. The thickness of the obtained glass was about 1 mm. According to the amount of MoS_2/ZnO added, the samples were denoted as $(MoS_2/ZnO)_4$/PMMA (4.0 mg), $(MoS_2/ZnO)_6$/PMMA (6.0 mg), and $(MoS_2/ZnO)_8$/PMMA (8.0 mg). For comparison, a MoS_2/PMMA organic glass was also fabricated according to the above process.[17, 28, 35]

2.3 NLA, NLS, and OL measurements of MoS_2/ZnO/PMMA organic glasses

The NLA and NLS properties of the $(MoS_2/ZnO)_{4–8}$/PMMA and $(MoS_2)_6$/PMMA organic glasses were investigated using a modified Z-scan technique.[35] The laser used in the measurements was an Nd:YAG laser system, which produced 6 ns laser pulses at 532 nm with a repetition rate of 1 Hz. The spatial distribution of the laser pulses exhibited a nearly Gaussian profile. The input and output energies of the laser pulses were measured by energy meters (Laser energy meter WIR-68254). The investigated samples were mounted on a mobile platform controlled by a computer that moved the sample along the z-axis through the focal plane of 150 mm focal length lens. The beam waist radius ($1/e^2$ radius) in the focal plane was 47 μm and the input energy was in the range of 13–66 μJ (the input peak light intensity at focus was in the range of 62.6–318 $MWcm^{-2}$), which was lower than the damage threshold of the organic glasses (~ 1.5 GW cm^{-2}). As for the OL measurement, the sample was fixed at z = –50 mm, where z = 0 corresponds to the focus of the lens. The input energy was in the range of 9–211 μJ, corresponding to the input fluence in the range of 0.13–3.04 J cm^{-2}.

3 Results and discussions

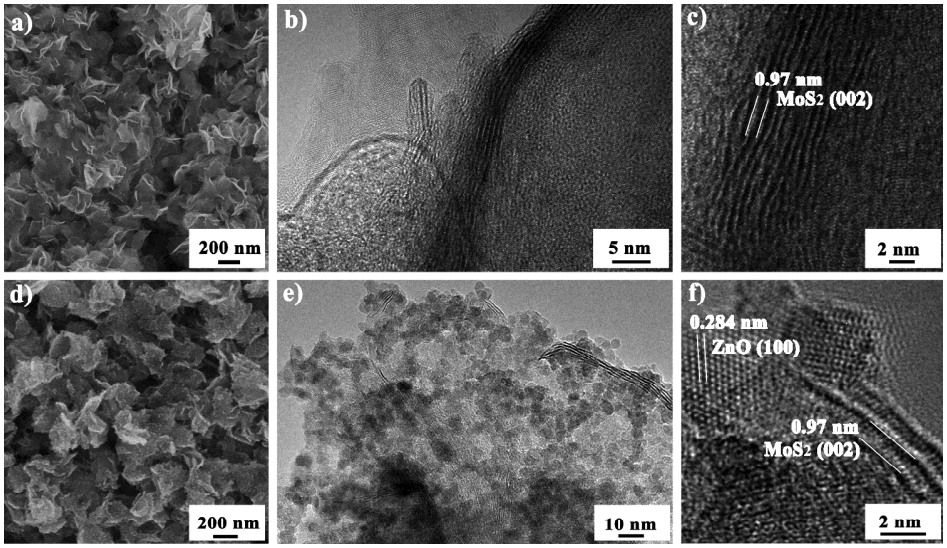

Fig. 1 Structural characterizations of MoS_2 nanosheets and MoS_2/ZnO composites. (a) SEM, (b) TEM, and (c) HRETEM images of MoS_2 nanosheets, and (d) SEM, (e) TEM, and (f) HRETEM images of MoS_2/ZnO composites.

The morphologies and size of the MoS_2 nanosheets and MoS_2/ZnO composites were characterized by scanning electron microscope (SEM) and transmission electron microscopy (TEM). Fig. 1(a) shows a typical SEM image of as-obtained MoS_2 nanosheets. It reveals that MoS_2 is of ultrathin nanosheet morphology with uniform lateral size of about 200 nm. TEM (Fig. 1(b)) shows that the basal plane of the MoS_2 nanosheets is very smooth, and their thicknesses are 5–10 nm. The cross-sectional high-resolution (HR) TEM image of the curled edges of the nanosheets demonstrates that the interlayer spacing of (002) crystal plane of the nanosheets is about 0.97 nm, as shown in Fig. 1(c). It suggests that the interlayer spacing of (002) crystal plane of the MoS_2 nanosheets is expanded compared to that of bulk MoS_2 (its interlayer spacing is about 0.615 nm). SEM image (Fig. 1(d)) shows that after ZnO loading the sample still exhibits nanosheet morphology. From the SME image, it can be also found that compared to the bare MoS_2 nanosheets, the MoS_2/ZnO composites have little change in lateral size; however, the basal planes of MoS_2 nanosheets become very rough. TEM observation (Fig. 1(e)) reveals that ZnO nanoparticles are adsorbed on the

basal planes of MoS_2 nanosheets. After measurments of more than 100 ZnO nanoparticles by TEM observation, we found that the ZnO nanoparticles have an average diameter of about 4.5 nm. HRTEM image (Fig. 1(f)) clearly shows the crystal nature of ZnO nanoparticles. The labeled lattice spacing for ZnO nanoparticles in the HRTEM image is about 0.284 nm, which can be attributed to (100) plane of hexagonal ZnO. Notably, HRTEM observation (Fig. 1(f)) reveals that the interlayer distance of (002) plane has not almost changed after ZnO coating because the coating is achieved at room temperature under very gentle conditions. Comparison of the high-magnification TEM images further confirms that crystalline ZnO nanoparticles are coated on the weakly crystalline basal surface of MoS_2 nanosheets, as shown in Fig. S1. The SEM images of the MoS_2/ZnO/PMMA organic glass confirm that MoS_2/ZnO composites with original structure can be dispersed in PMMA organic glass, as shown in Fig. S2.

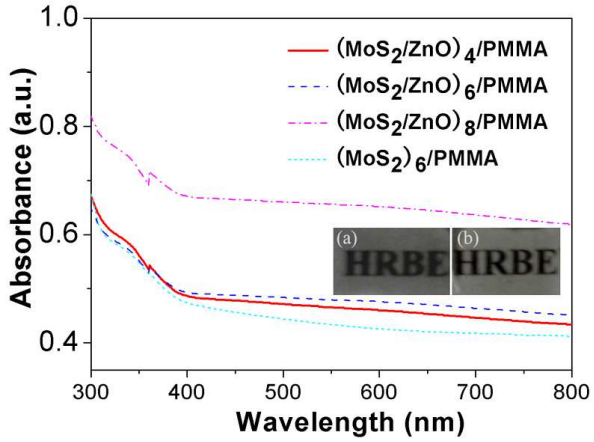

Fig. 2 UV-vis absorption spectra of $(MoS_2/ZnO)_4$/PMMA, $(MoS_2/ZnO)_6$/PMMA, $(MoS_2/ZnO)_8$/PMMA and $(MoS_2)_6$/PMMA organic glasses. The inset (a) and (b) are photographs of $(MoS_2/ZnO)_6$/PMMA and $(MoS_2)_6$/PMMA organic glasses, respectively.

UV-visible (UV-vis) absorption spectra of the $(MoS_2/ZnO)_{4–8}$/PMMA and $(MoS_2)_6$/PMMA organic glasses were measured by Shimadzu UV-2450 spectrometer, as shown in Fig. 2. In the wavelength range of 300–400 nm, these four samples have similar broad absorption peaks. The absorbance of the MoS_2/ZnO/PMMA organic glasses increases with increasing added amount of MoS_2/ZnO composites in organic glass. The $(MoS_2/ZnO)_8$/PMMA organic glass exhibits the strongest linear absorption. All absorbance of the $(MoS_2/ZnO)_{4–8}$/PMMA organic glasses are larger than that of the $(MoS_2)_6$/PMMA organic glass. This result implies that the MoS_2/ZnO/PMMA organic glasses may have better NLO properties.[35]

The linear absorption coefficient α_0 can be obtained from UV-vis spectra. In addition, near the band edge in the energy region of $h\nu < E_g$, α_0 empirically follows the exponential law:[37]

$$\alpha_0(\lambda) = A\exp(\frac{hc}{\lambda E_0}) \quad (1)$$

where A is a constant, h is the Planck's constant, λ is the wavelength, and E_0 is the Urbach energy which describing the width of the localized states in the band gap.[37, 38] Eq. (1) indicates that α_0 increases with the decreasing of E_0. Fig. 2 shows that the $(MoS_2/ZnO)_{4–8}$/PMMA organic glasses have larger absorbance which indicates that they have larger α_0 values. Therefore the MoS_2/ZnO/PMMA organic glasses have narrower localized states.

The inset (a) and (b) of Fig. 2 shows the photographs of the $(MoS_2/ZnO)_6$/PMMA and $(MoS_2)_6$/PMMA organic glasses, respectively. The ''HRBE'' letters underneath the glasses can be visualized by the naked eye, suggesting that both $(MoS_2/ZnO)_6$/PMMA and $(MoS_2)_6$/PMMA organic glasses organic glasses are transparent to visible light.

Fig. 3(a)–(d) show all Z-scan curves, which are plotted by the experimental data recorded by detectors D_a (NLA alone) and D_{sa} (NLA and NLS). The comparison of the NLA and NLS curves among $(MoS_2/ZnO)_4$/PMMA, $(MoS_2/ZnO)_6$/PMMA, and $(MoS_2/ZnO)_8$/PMMA organic glasses with the input energy of 66 μJ are shown in Fig. 3(a). From the figure, both dips in the D_a and D_{sa} curves of the $(MoS_2/ZnO)_4$/PMMA organic glass are the smallest, which are 0.47 and 0.38, respectively. However, the dips in the D_a and D_{sa} curves of the $(MoS_2/ZnO)_6$/PMMA organic glass are 0.41 and 0.18, respectively. The dips in the D_a and D_{sa} curves of the $(MoS_2/ZnO)_8$/PMMA organic glass are 0.42 and 0.25, respectively. The above results reveal that both NLA and NLS contribute to the NLO properties of the $(MoS_2/ZnO)_{4–8}$/PMMA organic glasses, and the $(MoS_2/ZnO)_6$/PMMA organic glass exhibit the best NLO properties.

Fig. 3(b) shows the comparison of the NLA and NLS curves between $(MoS_2/ZnO)_6$/PMMA and $(MoS_2)_6$/PMMA organic glasses with the input energy of 66 μJ. The dips in the D_a and D_{sa} curves of the $(MoS_2)_6$/PMMA organic glass are 0.48 and 0.47, respectively, which are smaller than those of the $(MoS_2/ZnO)_6$/PMMA organic glass. The compared results indicate that the MoS_2/ZnO/PMMA organic glasses exhibit enhanced NLO properties.

In order to explore the input energy dependence of NLA for the MoS_2/ZnO/PMMA organic glasses, the samples are scanned at the same position with increasing and decreasing the input energy. Fig. 3(c) and (d) show the NLA curves of the $(MoS_2/ZnO)_6$/PMMA and $(MoS_2)_6$/PMMA organic glasses with the input energies of 13–51 μJ. At the input energy of 13 μJ, there are no transmission variations for both $(MoS_2/ZnO)_6$/PMMA and $(MoS_2)_6$/PMMA organic glasses. At the input energies of 19 and 20 μJ, both of them exhibit an increase of transmittance at positions close to the focus, a typical SA effect. In addition, for the same sample, the peak of the NLA curve with the input energy of 19 μJ is higher. When the input energy is increased to be 21 μJ, both $(MoS_2/ZnO)_6$/PMMA and $(MoS_2)_6$/PMMA organic glasses begin to exhibit a changeover from SA to RSA. When the input energy is continually increased to be 23, 32 and 41 μJ, both $(MoS_2/ZnO)_6$/PMMA and $(MoS_2)_6$/PMMA organic glasses still exhibit a changeover from SA to RSA, and the higher input energy corresponds to the deeper valley at focus. As the input energy is increased to be 51 μJ, both $(MoS_2/ZnO)_6$/PMMA and $(MoS_2)_6$/PMMA organic glasses completely changes from SA to RSA.

In order to obtain the NLA and NLS coefficients, the experimental data are firstly analyzed by a model related to SA, RSA, and NLS.[16, 39, 40] The total extinction coefficient $\alpha(I)$ can be expressed as: [16, 39, 40]

$$\alpha(I) = \frac{\alpha_0}{1 + I / I_s} + \beta_1 I \quad , \tag{2}$$

where α_0 is the linear absorption coefficient, I is the laser light intensity, I_s is the saturation light intensity, and β_1 is total nonlinear extinction coefficient ($\beta_1 = \beta_{1A} + \beta_{1S}$). β_1 and β_{1A} can be obtained from D_{sa} and D_a, respectively, and correspondingly β_{1S} can also be extracted. Therefore the modified normalized transmittance using Eq. (2) can be written as:[16, 39]

$$T(z) = \frac{Q(z)}{\sqrt{\pi} q(z)} \int_{-\infty}^{+\infty} \ln\left[1 + q(z)\exp(-\tau^2)\right] d\tau \quad . \tag{3}$$

where

$$Q(z) = \exp\left[\alpha_0 LI/(I + I_s)\right]$$
$$q(z) = \beta_1 I_0 L_{eff} / (1 + z^2 / z_0^2) \quad . \tag{4}$$

I_0 is the peak light intensity at focus; $L_{eff} = [1–\exp(–\alpha_0 L)]/\alpha_0$ is the effective thickness of the sample; L is the thickness of the sample (L = 1 mm for all samples in this work). $z_0 = \pi w_0^2/\lambda$ is the Rayleigh range, where w_0 is the beam waist radius; and λ is the wavelength of the incident light.

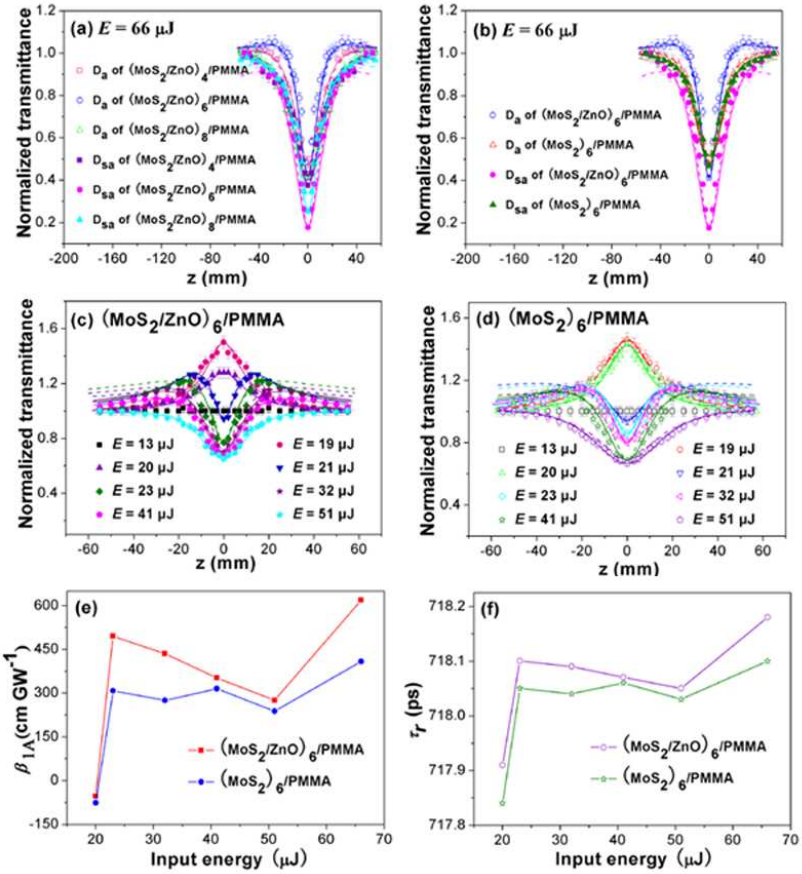

Fig. 3 The comparison of NLA and NLS curves (a) among $(MoS_2/ZnO)_4$/PMMA, $(MoS_2/ZnO)_6$/PMMA, and $(MoS_2/ZnO)_8$/PMMA; and (b) between $(MoS_2/ZnO)_6$/PMMA and $(MoS_2)_6$/PMMA organic glasses with the input energy of 66 μJ. The NLA curves of (c) $(MoS_2/ZnO)_6$/PMMA and (d) $(MoS_2)_6$/PMMA organic glasses with different input energies. The comparison of (e) β_{1A} and (f) τ_r values via the input energy between $(MoS_2/ZnO)_6$/PMMA and $(MoS_2)_6$/PMMA organic glasses. All solid lines and dashed lines in Fig. 3(a)–(d) are fitting curves using Eq. (2)–(4) and Eq. (5)–(6), respectively.

Table 1 The comparison for β_1, β_{1A}, β_{1S}, and I_s (obtained according to Eq. (2)–(4)), β_2, β_{2A}, β_{2S}, and τ_r (obtained according to Eq. (5) and (6)) among $(MoS_2/ZnO)_4$/PMMA, $(MoS_2/ZnO)_6$/PMMA, $(MoS_2/ZnO)_8$/PMMA, and $(MoS_2)_6$/PMMA organic glasses with the input energy of 66 μJ

Samples	β_1 (cm GW^{-1})	β_{1A} (cm GW^{-1})	β_{1S} (cm GW^{-1})	I_s (MW cm^{-2})	β_2 (cm GW^{-1})	β_{2A} (cm GW^{-1})	β_{2S} (cm GW^{-1})	τ_r (ps)
$(MoS_2/ZnO)_4$/PMMA	675	458	217	27.2	386	318	68	718.12
$(MoS_2/ZnO)_6$/PMMA	2380	618	1762	16.2	352	312	40	718.18
$(MoS_2/ZnO)_8$/PMMA	1920	828	1092	27.2	498	475	23	718.18
$(MoS_2)_6$/PMMA	418	408	10	35.2	378	308	70	718.10

The solid lines in Fig. 3(a)–(d) are the fitting curves using Eq. (2)–(4). The values of linear transmittance T_0 and α_0 at λ = 532 nm of the $(MoS_2/ZnO)_4$/PMMA, $(MoS_2/ZnO)_6$/PMMA, $(MoS_2/ZnO)_8$/PMMA, and $(MoS_2)_6$/PMMA organic glasses

obtained from UV-vis spectra are 62.6%, 61.8%, 51.8%, 64.6%, 4.68 cm^{-1}, 4.81 cm^{-1}, 6.57 cm^{-1}, and 4.37 cm^{-1}, respectively. According to Eq. (2)–(4), the fitting NLO parameters (β_1, β_{1A}, β_{1S}, and I_s) of the $(MoS_2/ZnO)_{4-8}$/PMMA and $(MoS_2)_6$/PMMA organic glasses with the input energy of 66 μJ can be obtained and listed in Table 1. From Table 1, it can be seen that all β_1, β_{1A}, and β_{1S} values of the $(MoS_2/ZnO)_{4-8}$/PMMA organic glasses are larger than those of the $(MoS_2)_6$/PMMA organic glass. The β_1, β_{1A}, and β_{1S} values of the $(MoS_2/ZnO)_6$/PMMA organic glass are approximately 5.7, 1.5, and 176.2 times larger than those of the $(MoS_2)_6$/PMMA organic glass, respectively. However, the I_s value of the $(MoS_2)_6$/PMMA organic glass is the largest.

The calculated values of β_{1A} and I_s of the $(MoS_2/ZnO)_6$/PMMA and $(MoS_2)_6$/PMMA organic glasses with different input energies are listed in Table 2 and 3, respectively. From Table 2 and 3, it can be seen that the β_{1A} values both of $(MoS_2/ZnO)_6$/PMMA and $(MoS_2)_6$/PMMA organic glasses firstly increase, and then decreases and again increases with the increasing of the input energy. At the input energy of 19 and 20 μJ, the β_{1A} values are negative, while the β_{1A} values are positive at other input energies, as shown in Fig. 3 (e). It is obviously that the β_{1A} value of the $(MoS_2/ZnO)_6$/PMMA organic glass is larger than that of the $(MoS_2)_6$/PMMA organic glass at the same input energy.

Table 2 The values of β_{1A} and I_s of the $(MoS_2/ZnO)_6$/PMMA organic glass with different input energies obtained according to Eq. (2)–(4), and the values of β_{2A} and τ_r obtained according to Eq. (5) and (6).

E (μJ)	β_{1A} (cm GW^{-1})	I_s (MW cm^{-2})	β_{2A} (cm GW^{-1})	τ_r (ps)
19	–89.5	428	1650	717.85
20	–53.2	521	1670	717.91
21	315	5.25	1200	718.06
23	495	5.25	1110	718.10
32	435	9.95	821	718.09
41	352	19.2	658	718.07
51	275	64.2	568	718.05
66	618	16.2	312	718.18

Table 3 The values of β_{1A} and I_s of the $(MoS_2)_6$/PMMA organic glass with different input energies obtained according to Eq. (2)–(4), and the values of β_{2A} and τ_r obtained according to Eq. (5) and (6).

E (μJ)	β_{1A} (cm GW^{-1})	I_s (MW cm^{-2})	β_{2A} (cm GW^{-1})	τ_r (ps)
19	–90.2	798	1620	717.83
20	–76.4	462	1530	717.84
21	248	12.3	1180	718.04
23	308	11.2	1080	718.05
32	275	12.5	768	718.04
41	318	12.5	545	718.06
51	242	49.8	495	718.03
66	408	35.2	308	718.10

In order to investigate the NLO dynamic process of the MoS_2/ZnO/PMMA organic glasses, the energy-level diagram of the MoS_2/ZnO composites is given as shown in Fig. 4. Because no NLO properties are observed in PMMA, the energy level diagram of the MoS_2/ZnO composites can be used to analyze the photodynamic processes in the MoS_2/ZnO/PMMA organic glasses.[17, 28, 35] In Fig. 4, the valence band (VB) and conduction band (CB) of ZnO nanorods are defined at –7.39 and –4.19 eV on the absolute vacuum scale (AVS), respectively.[34] Because of the small size effect of ZnO nanoparticles, their actual energy levels of VB and CB are at –7.56 and –4.02 eV, respectively.[28] Because the band gap of MoS_2 is in the range of 1.2–1.9 eV,[3, 4, 16] and the top of VB and the bottom of VB of MoS_2 are near –1.0 and 1.0 eV,[41] respectively, therefore the energy levels of the MoS_2 nanosheets are shown in Fig. 4.[16]

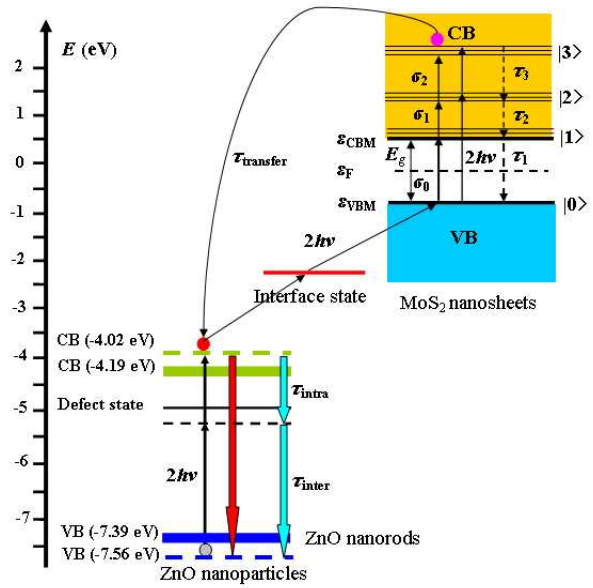

Fig. 4 Energy level diagram of MoS_2/ZnO composites.

According to the energy level diagram, when irradiated by 6 ns laser pulses at 532 nm, the photodynamic processes in the MoS_2/ZnO/PMMA organic glasses involve: (1) electron transition from VB to CB of ZnO nanoparticles through two-photon absorption (2PA). The excited electrons will relax from CB to VB by interband transition, or they can first be trapped by defect state or surface state and then return to VB;[34] (2) interband transition and intraband transition in MoS_2 nanosheets through one-photon absorption (1PA), i.e |0>→|1>, |1>→|2> and |2>→|3>; (3) electron transition from |0> state to |2> state through 2PA and from |2> state to |3> state through 1PA in MoS_2 nanosheets. The excited electrons will firstly relax from |3> state to |2> state and then return to |0> state; and (4) interfacial charge transfer process from |3> state in MoS_2 nanosheets to the bottom of CB in ZnO nanoparticles.[28] The excess electrons in CB of ZnO nanoparticles can firstly jump to the interface state and then transfer back to MoS_2 nanosheets through 2PA.

For the nanosecond laser, the pulse width is much longer than the intraband relaxation time in ZnO nanoparticles and MoS_2 nanosheets (τ_{intra}, τ_2 and τ_3 are on the order of femtoseconds).[16, 41, 42] Hence the equations governing the NLO process in the nanosecond regime can be expressed as:[16, 35]

$$\frac{\partial I}{\partial z'} = -(\alpha_0 + N_{ex}\sigma_{eff} + \beta_2 I)I \quad , \qquad (5)$$

$$\frac{\partial N_{ex}}{\partial t} = \frac{\alpha_0 I}{h\nu} - \frac{N_{ex}}{\tau_r} + \frac{\beta_{2A} I^2}{2h\nu} . \quad (6)$$

where N_{ex} is the effective excited carrier density (the ground-state carrier density is denoted as N_0), and $h\nu$ is photon energy (2.33 eV); σ_{eff} is the effective free carrier absorption (FCA) cross section, α_0 and β_{2A} are the linear absorption and effective 2PA coefficient, respectively; β_2 is total nonlinear extinction coefficient ($\beta_2 = \beta_{2A} + \beta_{2S}$). β_2 and β_{2A} can be obtained from D_{sa} and D_a, respectively, and correspondingly β_{2S} can also be extracted. τ_r is the effective relaxation time, which is related to the interband relaxation time τ_{inter} and τ_1 (several hundred picoseconds),[16, 42] and charge transfer time $\tau_{transfer}$ from MoS_2 nanosheets to ZnO nanoparticles; z' is the coordinate inside the nonlinear sample which changes from zero to L, and L is the thickness of sample. I is the laser light intensity.

According to Eq. (5) and (6), we used the four-order Runge-Kutta method to fit the experimental data of the $(MoS_2/ZnO)_{4-8}$/PMMA and $(MoS_2)_6$/PMMA organic glasses. The dashed lines in Fig. 3(a)–(d) show the fitting results. During the fitting processes, the σ_{eff} value is fixed as 3.04×10^{-21} m^2 for all samples.[16, 35] The N_0 values of the $(MoS_2/ZnO)_4$/PMMA, $(MoS_2/ZnO)_6$/PMMA, $(MoS_2/ZnO)_8$/PMMA, and $(MoS_2)_6$/PMMA organic glasses are 2.541×10^{25}, 2.553×10^{25}, 2.555×10^{25}, and 2.533×10^{25} m^{-3}, respectively. According to Eq. (5) and (6), the values of β_{2A} and τ_r of the $(MoS_2/ZnO)_{4-8}$/PMMA and $(MoS_2)_6$/PMMA organic glasses with the input energy of 66 μJ can be firstly obtained from the fitting results based on the D_a data, and listed in Table 1. Then, the above parameters are substituted in Eq. (5) and (6), β_2 can be obtained from the fitting results in terms of the D_{sa} data, and consequently β_{2S} is also obtained. Because the contributions of the higher states |2> and |3> to the NLA are neglected, the values of β_2 and β_{2A} are smaller than those of β_1 and β_{1A}, respectively. In addition, all β_{2A} and τ_r values of the $(MoS_2/ZnO)_{4-8}$/PMMA organic glasses are larger than those of the $(MoS_2)_6$/PMMA organic glass. Besides, all β_2 and β_{2A} values of the $(MoS_2/ZnO)_{4-8}$/PMMA organic glasses are larger than those of the $ZnO_{7.8}$/PMMA organic glass (197 and 148 cm GW^{-1}).[28]

The β_{2A} and τ_r values of the $(MoS_2/ZnO)_6$/PMMA and $(MoS_2)_6$/PMMA organic glasses with different input energies are listed in Table 2 and 3, respectively. For both $(MoS_2/ZnO)_6$/PMMA and $(MoS_2)_6$/PMMA organic glasses, the β_{2A} values decreases with increasing input energy, which is due to the saturation of RSA.[16, 35] In addition, the β_{2A} value of the $(MoS_2/ZnO)_6$/PMMA organic glass is larger than that of the $(MoS_2)_6$/PMMA organic glass at the same input energy, which further confirms that the MoS_2/ZnO/PMMA organic glasses exhibit enhanced NLO properties.

The comparison of τ_r values via input energy between $(MoS_2/ZnO)_6$/PMMA and $(MoS_2)_6$/PMMA organic glasses is shown in Fig. 3 (f). At the same input energy, the τ_r value of the $(MoS_2/ZnO)_6$/PMMA organic glass is larger than that of the $(MoS_2)_6$/PMMA organic glass. In addition, for both $(MoS_2/ZnO)_6$/PMMA and $(MoS_2)_6$/PMMA organic glasses, when the input energy is lower, the τ_r values are smaller, i.e. the excited carriers can quickly return back to the ground-state or the top of VB, the ground-state absorption plays a dominant role, therefore the samples exhibit SA. While the input energy is higher, the τ_r values become larger, i.e. the excited carriers slowly return back to the ground-state or the top of VB, the excited-state absorption plays a dominant role, leading to the changeover from SA to RSA or complete RSA.[16]

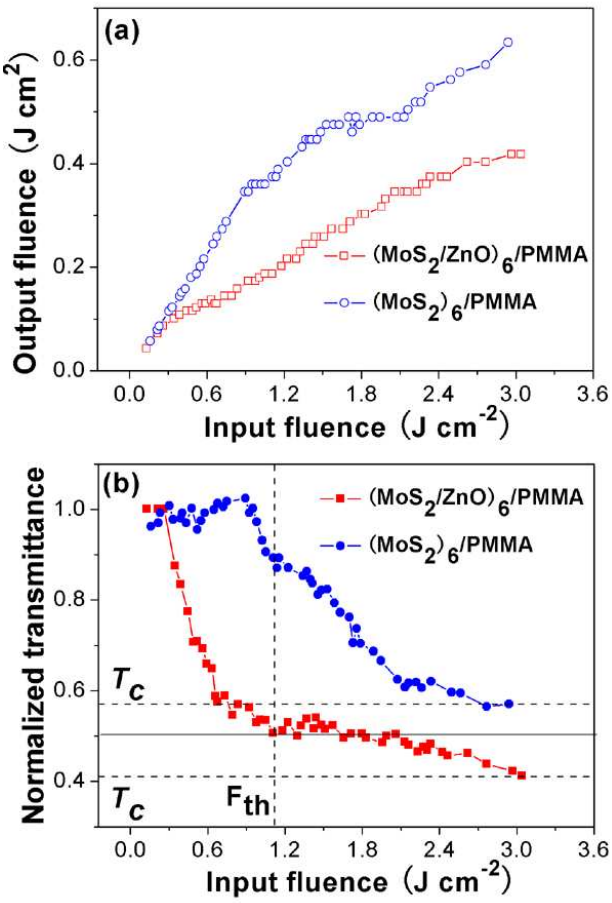

Fig. 5 The comparison of OL curves between $(MoS_2/ZnO)_6$/PMMA and $(MoS_2)_6$/PMMA organic glasses, (a) the output fluence and (b) the normalized transmittance via the input fluence.

The above results demonstrate that the $(MoS_2/ZnO)_6$/PMMA organic glass exhibits the best NLA and NLS properties, suggesting that it should have excellent OL performance. Fig. 5 shows the comparison of optical limiting (OL) curves between $(MoS_2/ZnO)_6$/PMMA and $(MoS_2)_6$/PMMA organic glasses. Fig. 5 (a) and (b) show the variation of the output fluence and the normalized transmittance as the function of the input fluence, respectively. From Fig. 5(a), it can be seen that when the input fluence is 2.26 J cm^{-2}, the output fluence of the $(MoS_2)_6$/PMMA organic glass increases sharply, indicating that the sample is damaged. While the $(MoS_2/ZnO)_6$/PMMA organic glass is not damaged. From Fig. 5(b), The OL threshold F_{th} (defined as the input fluence at the normalized transmittance of 0.5) and clamping normalized transmittance T_c of the $(MoS_2/ZnO)_6$/PMMA organic glass are 1.11 J cm^{-2} and 0.41, respectively. However, the F_{th} and T_c values of the $(MoS_2)_6$/PMMA organic glass are > 1.11 J cm^{-2} and 0.56, respectively. The above results show that the $(MoS_2/ZnO)_6$/PMMA organic glass exhibits better OL

performance.

The enhanced NLO and OL properties of the MoS_2/ZnO/PMMA organic glasses can be attributed to the interfacial charge transfer between MoS_2 nanosheets and ZnO nanoparticles, which can suppress the recombination between electrons and holes, which will result in larger charge carrier lifetime.[8, 28] Furthermore, the layered structure of MoS_2 nanosheets can afford not only larger surface areas to absorb light but also higher in-plane carrier mobility, which can result in significant enhancement of NLO and OL properties.[17] The abundance of defect or surface states induced by the small size effect of ZnO nanoparticles will become scattering centres, resulting in stronger NLS.[28] The enhanced linear and nonlinear absorption of the MoS_2/ZnO/PMMA organic glasses may lead to thermal accumulation of absorbed laser, which is useful for the formation of carbon vapor bubbles. The formed carbon vapor bubbles as optical scattering centres[43] can also result in stronger NLS.[44] The narrower local states in the band gap of the MoS_2/ZnO/PMMA organic glasses can increase the electron transition, which consequently resulting in enhanced NLO and OL properties.[39] According to the local field effect, the total nonlinear extinction coefficient of the MoS_2/ZnO/PMMA organic glasses can be expressed as:[45]

$$\beta_{composite(1\ or\ 2)} = \frac{\beta_{\text{single (1 or 2)}}}{f^4 v_f}. \quad (7)$$

where $\beta_{\text{single (1 or 2)}}$ is the total nonlinear extinction coefficient of the MoS_2/PMMA or ZnO/PMMA organic glasses, f is the local field factor ($f = (n_0^2 + 2)/3$, n_0 is the linear refraction index of the PMMA), and v_f is the volume fraction of MoS_2 or ZnO relative to the MoS_2/ZnO/PMMA organic glasses. The n_0 value of PMMA is in the range of 1.482–1.521. If n_0 is taken as 1.5, and the β_2 value of the $(MoS_2/ZnO)_8$/PMMA organic glass (498 cm/GW) is approximately 2.5 times larger than that of the $ZnO_{7.8}$/PMMA organic glass (197 cm/GW),[28] the v_f value of ZnO in the $(MoS_2/ZnO)_8$/PMMA organic glass can be calculated as about 9.7%.

Compared to the MoS_2 films, although the NLA coefficients β_{1A} and β_{2A} of the MoS_2/ZnO/PMMA organic glasses are smaller than those of the former, the MoS_2/ZnO/PMMA organic glasses have higher optical damage threshold, better mechanical strength and flexibility. The deformation of the MoS_2/ZnO/PMMA organic glass can be up to 2.82 mm, which is much larger than that of the slide glass (0.23 mm), as shown in Fig. S3. The optical damage threshold MoS_2/ZnO/PMMA organic glasses is 1.5 GW cm^{-2}, while the optical damage threshold of the MoS_2 films is 400 MW cm^{-2}, the former is approximately 3.8 times larger than the latter. The MoS_2/ZnO/PMMA organic glasses can bear the struck of the iron hammer with the weight of about 500 g. In addition, the MoS_2/ZnO/PMMA organic glasses can be cut into different sizes and shapes according to the practical applications.

4 Conclusions

MoS_2/ZnO composites were synthesized by a solution-based method, and MoS_2/ZnO/PMMA organic glasses were fabricated by a casting method. The NLA and NLS properties of the MoS_2/ZnO/PMMA organic glasses were investigated by using a modified Z-scan technique. The experimental results indicated that both NLA and NLS contributed to the NLO properties. The MoS_2/ZnO/PMMA organic glasses exhibited SA and the changeover from SA to RSA by adjusting the input energy. The experimental data were simulated by using the modified Z-scan theory and simplified rate equations. The NLO dynamic process of the MoS_2/ZnO/PMMA organic glasses has been analyzed by applying the energy-level model of MoS_2/ZnO composites. Compared to MoS_2/PMMA and ZnO/PMMA organic glasses, the MoS_2/ZnO/PMMA organic glasses exhibited enhanced NLO properties, which were attributed to the interfacial charge transfer between MoS_2 nanosheets and ZnO nanoparticles, the layered structures of MoS_2 nanosheets, the small size effect of ZnO nanoparticles, and the local field effect. The better NLO properties, fast response time, higher optical damage threshold, better mechanical strength and flexibility make the MoS_2/ZnO/PMMA organic glasses very promising for optical devices such as optical limiters, optical shutters, ultrafast lasers, and ultrafast optical switches.

Acknowledgements

This work was supported by the National Natural Science Fund of China (Grant Nos. 61205113, 51272050, and 51302047), the Innovation Foundation of Harbin City (2012RFXXG096), and also the 111 project (B13015) of Ministry Education of China to the Harbin Engineering University.

Notes and references

[a] *Key Laboratory of In-Fiber Integrated Optics of Ministry of Education, College of Science, Harbin Engineering University, Harbin 150001, China.*
E-mail: chenyujin@hrbeu.edu.cn and qyouyang7823@aliyun.com
[b] *Department of Applied Chemistry, College of Science, Northeast Agricultural University, Harbin 150030, China*

† Electronic Supplementary Information (ESI) available: [Comparison of the high-magnification TEM images of MoS_2 between MoS_2/ZnO]. See DOI: 10.1039/b000000x/

1 C. Ataca, H. Şahin and S. Ciraci, *J. Phys. Chem. C*, 2012, **116**, 8983–8999.
2 Q. H. Wang, K. Kalantar-Zadeh, A. Kis, J. N. Coleman and M. S. Strano, *Nat. Nanotechnol.*, 2012, **7**, 699–712.
3 C. Lee, H. Yan, L.E. Brus, T.F. Heinz, J. Hone and S. Ryu, *ACS Nano*, 2010, **4**, 2695–2700.
4 K. F. Mak, C. Lee, J. Hone, J. Shan and T. F. Heinz, *Phys. Rev. Lett.* 2010, **105**, 136805.
5 Y. H. Tan, K. Yu, T. Yang, Q. F. Zhang, W. T. Cong, H. H. Yin, Z. L. Zhang, Y. W. Chen and Z. Q. Zhu, *J. Mater. Chem. C*, 2014, **2**, 5422–5430.
6 Y. H. Tan, K. Yu, J. Z. Li, H. Fu and Z. Q. Zhu, *J. Appl. Phys.*, 2014, **116**, 064305.
7 W. J. Zhou, Z. Y. Yin, Y. P. Du, X. Huang, Z. Y. Zeng, Z. X. Fan, H. Liu, J. Y. Wang and H. Zhang, *Small*, 2013, **9**, 140–147.
8 Q. J. Xiang, J. G. Yu and M. Jaroniec, *J. Am. Chem. Soc.*, 2012, **134**, 6575–6578.
9 X. Zong, H. J. Yan, G. P. Wu, G. J. Ma, F. Y. Wen, L. Wang and C. Li, *J. Am. Chem. Soc.*, 2008, **130**, 7176–7177.
10 A. Splendiani, L. Sun, Y. Zhang, T. Li, J. Kim, C. Y. Chim, G. Galli and F. Wang, *Nano Lett.*, 2010, **10**, 1271–1275.
11 G. Eda, H. Yamaguchi, D. Voiry, T. Fujita, M. Chen and M. Chhowalla, *Nano Lett.*, 2011, **11**, 5111–5116.
12 G. L. Frey, K. J. Reynolds, R. H. Friend, H. Cohen and Y. Feldman, *J. Am. Chem. Soc.*, 2003, **125**, 5998–6007.

13 H. S. Lee, S. W. Min, Y. G. Chang, M. K. Park, T. Nam, H. Kim, J. H. Kim, S. Ryu and S. Im, *Nano Lett.*, 2012, **12**, 3695−3700.

14 Z. Y. Yin, H. Li, H. Li, L. Jiang, Y. M. Shi, Y. H. Sun, G. Lu, Q. Zhang, X. D. Chen and H. Zhang, *ACS Nano*, 2012, **6**, 74–80.

15 W. Choi, M. Y. Cho, A. Konar, J. H. Lee , G. B. Cha , S. C. Hong , S. Kim, J. Kim , D. Jena , J. Joo and S. Kim, *Adv. Mater.*, 2012, **24**, 5832–5836.

16 Q. Y. Ouyang, H. L. Yu, K. Zhang and Y. J. Chen, *J. Mater. Chem. C*, 2014, **2**, 6319–6325.

17 Q. Y. Ouyang, H. L. Yu, H. Y. Wu, Z. Y. Lei, L. H. Qi and Y. J. Chen, *Opt. Mater.*, 2013, **35**, 2352–2356.

18 H. Zhang, S. B. Lu, J. Zheng, J. Du, S. C. Wen, D. Y. Tang and K. P. Loh, *Opt. Express*, 2014, **22**, 7249–7260.

19 K. P. Wang, J. Wang, J. T. Fan, M. Lotya, A. O'Neill, D. Fox, Y. Y. Feng, X. Y. Zhang, B. X. Jiang, Q. Z. Zhao, H. Z. Zhang, J. N. Coleman, L. Zhang and W. J. Blau, *ACS Nano*, 2013, **7**, 9260–9267.

20 A. Dashora, U. Ahuja and K. Venugopalan, *Comp. Mater. Sci.*, 2013, **69**, 216–221.

21 S. K. Srivastava and D. Palit, *Solid State Ionics*, 2005, **176**, 513–521.

22 K. Chang and W. X. Chen, *ACS Nano*, 2011, **5**, 4720–4728.

23 G. T. Yue, J. H. Wu, Y. M. Xiao, M. L. Huang, J. M. Lin and J. Y. Lin, *J. Mater. Chem. A*, 2013, **1**, 1495–1501.

24 J. Z. Wang, L. Lu, M. Lotya, J. N. Coleman, S. L. Chou, H. K. Liu, A. I. Minett and J. Chen, *Adv. Energy Mater.*, 2013, **3**, 798–805.

25 Y. Liu, Y. X. Yu and W. D. Zhang, *J. Phys. Chem. C*, 2013, **117**, 12949–12957.

26 L. Y. Gan, Q. Y. Zhang, Y. C. Cheng and U. Schwingenschlögl, *J. Phys. Chem. Lett.*, 2014, **5**, 1445–1449.

27 M. A. M. Versteegh and J. I. Dijkhuis, *Opt. Lett.*, 2011, **36**, 2776–2778.

28 Q. Y. Ouyang, Z. Xu, Z. Y. Lei, H. W. Dong, H. L. Yu, L. H. Qi, C. Y. Li and Y. J. Chen, *Carbon*, 2014, **67**, 214–220.

29 L. Irimpan, B. Krishnan, V. P. N. Nampoori and P. Radhakrishnan, *Appl. Opt.*, 2008, **47**, 4346–51.

30 B. Krishnan, L. Irimpan, V. P. N. Nampoori and V. Kumar, *Phys. E*, 2008, **40**, 2787–2790.

31 S. C. Li, K. Yu, Y. Wang, Z. L. Zhang, C. Q. Song, H. H. Yin, Q. Ren and Z. Q. Zhu, *CrystEngComm*, 2013, **15**, 1753–1761**.**

32 Y. Wang, S. C. Li, H. Shi and K. Yu, *Nanoscale*, 2012, 4, 7817–7824.

33 Z. Yang, L. J. Guo, B. Y. Zu, Y. A. Guo, T. Xu and X. C. Dou, Adv. *Opt. Mater.*, 2014, **2**, 738–745.

34 L. J. Tzeng, C. L. Cheng and Y. F Chen, *Opt. Lett.*, 2008, **33**, 569–571.

35 Q. Y. Ouyang, H. L. Yu, Z. Xu, Y. Zhang, C. Y. Li, L. H. Qi and Y. J. Chen, *Appl. Phys. Lett.*, 2013, **102**, 031912.

36 J. F. Xie, J. J. Zhang, S. Li, F. Grote, X. D. Zhang, H. Zhang, R. X. Wang, Y. Lei, B. C. Pan and Y. Xie, *J. Am. Chem. Soc.*, 2013, **135**, 17881−17888.

37 F. Yakuphanoglu, M. Sekerci and O.F. Ozturk, *Opti. Commun.*, 2004, **239**, 275–280.

38 Y. B. Han, J. B. Han, S. Ding, D. J. Chen and Q. Q. Wang, *Opt. Express*, 2005, **13**, 9211–9216.

39 P. A. Kurian, C. Vijayan, K. Sathiyamoorthy, C. S. SuchandSandeep and R. Philip, *Nanoscale Res. Lett.*, 2007, **2**, 561–568.

40 M. Hari, S. Mathew, B. Nithyaja, S. A. Joseph, V. P. N. Nampoori and P. Radhakrishnan, *Opt. Quantum Electron.*, 2012, **43**, 49–58.

41 A. Kumar, J. Kumar and P. K. Ahluwalia, *AIP Conf. Proc.*, 2012, **1447**, 1269–1270.

42 F. Wun, A. H. Liu, H. Zheng, H. T. Chang, P. Shi, K. X. Cheng and X. M. Cheng, *Phys. E*, 2012, **44**, 1158–1161.

43 Z. B. Liu, Y. F. Xu, X. Y. Zhang, X. L. Zhang, Y. S. Chen and J. G. Tian. *J. Phys. Chem. B* 2009,**113**, 9681–9686.

44 M. Feng, H. B. Zhan and Y. Chen. *Appl. Phys. Lett.* 2010, **96**, 033107.

45 H. I. Elim, W. Ji, L. Tian, M. T. Ng and J. J. Vittal, *Proc. SPIE*, 2007, **6639**, 663903.